Applied Surface Science 311 (2014) 837–841

Contents lists available at ScienceDirect

Applied Surface Science

journal homepage: www.elsevier.com/locate/apsusc

Temperature change effect on $BaTiO_3$ single crystal surface potential around domain walls

D.Y. He[a,b], X.R. Xing[b], L.J. Qiao[a,*], Alex A. Volinsky[c]

[a] Corrosion and Protection Center, Key Laboratory for Environmental Fracture (MOE), University of Science and Technology Beijing, Beijing 100083, People's Republic of China
[b] Department of Physical Chemistry, University of Science and Technology Beijing, Beijing 100083, People's Republic of China
[c] Department of Mechanical Engineering, University of South Florida, Tampa, FL 33620, USA

ARTICLE INFO

Article history:
Received 15 April 2014
Accepted 24 May 2014
Available online 2 June 2014

Keywords:
Ferroelectrics
Domain wall
Surface potential
Temperature effect

ABSTRACT

Temperature dependence of the surface potential distribution on the $BaTiO_3$ (0 0 1) single crystal ferroelectric domain walls was investigated by the scanning Kelvin probe microscopy. After decreasing the single crystal temperature below the Curie point (T_C), high potential (~600 mV) stripes were immediately observed near the 90° ***a*–*c*** domain wall surface. The potential stripes were not stable and decayed with time. The adjacent ***c*** domain surface screening charges and their mobility play a dominant role in this experiment. The corrugation topography at the 90° ***a*–*c*** domain wall acts as a natural charge trap and should not be neglected. Besides, the polarization and the strain variations across the wall induce large physical changes of the material.

1. Introduction

In ferroelectrics, domain walls separate domains with different polarizations, playing an important role in ferroelectric performance and the design of future electronic devices [1]. Domain walls physical properties, such as the electrical conductivity, magnetic properties and the atomic structure have attracted a widespread interest in recent years [2–5]. Dynamic studies of the domain walls have also been carried out [6–9]. Ferroelectric domain walls are only 2–4 nm wide [10–14]. Additionally, with the electric dipole direction change across the domain wall, the polarization and the strain also change [15]. Understanding domain wall behavior is crucial for ferroelectrics promising applications, particularly in nonvolatile memory, microwave ceramics, electromechanical sensors and actuators [1], and other such systems.

As a convenient, nondestructive and high resolution technique, the scanning probe microscopy (SPM) provides a powerful method for observing domain structures and their dynamic behavior at the micron and nanometer scales [16–23], enabling direct domain wall dynamics studies. Among the SPM modes, scanning Kelvin probe microscopy (SKPFM) is sensitive to electrostatic forces, and can be directly used to detect surface potential distribution on ferroelectric surfaces in-situ [24,25], which is useful for characterizing the ferroelectric domain wall performance.

2. Experiment

Here, a direct observation of the domain wall behavior was performed, while controllably cooling the $BaTiO_3$ (0 0 1) single crystal. An obvious high potential zone was observed at the 90° ***a*–*c*** domain wall. In this case, the change of temperature induced the fine tilt of the domain polarization [26], thus straining the domain wall areas. The polarization and strain changes across the wall induce physical change of the material that can not be ignored. The screening charge migration at the ferroelectric surface after temperature variation would also lead to a large charge trapped at the mismatched domain wall zone. The decay of the surface potential barrier gave an evidence for the surface charge migration. The corrugation topography at the 90° ***a*–*c*** domain wall, which acts as a charge trap, should not be neglected.

Commercial zero degree cut, undoped $BaTiO_3$ single crystal with ⟨0 0 1⟩ orientation and $5 \times 5 \times 1\ mm^3$ dimensions was used here for in situ imaging. The crystal was transparent and colorless. The sample preparation was as follows: first, the crystals were poled along the [1 0 0] direction to get the ***a*** domain on the (0 0 1) observed plane, and then the (0 0 1) surface was polished carefully by diamond lapping pastes and a 50 nm colloidal silica suspension until the (0 0 1) surface roughness was less than 1 nm. The sample was then cleaned supersonically in deionized water for 100 s. The Curie

* Corresponding author: Tel.: +86 10 6233 4499; fax: +86 10 6233 2345.
E-mail addresses: lqiao@ustb.edu.cn (L.J. Qiao), volinsky@usf.edu (A.A. Volinsky).

http://dx.doi.org/10.1016/j.apsusc.2014.05.175
0169-4332/

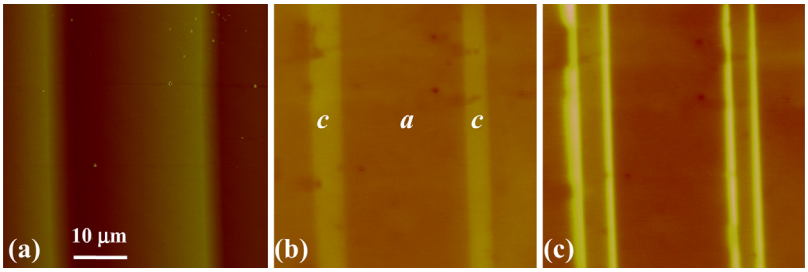

Fig. 1. (a) AFM topography image of the 90° ***a***– ***c*** domain structure on the (0 0 1) $BaTiO_3$ surface (200 nm Z scale); (b) corresponding surface potential image captured at 115 °C (0.6 V Z scale); (c) surface potential image captured immediately after cooling to 90 °C showing a higher potential barrier at the 90° ***a***– ***c*** domain wall (0.6 V Z scale). The potential barrier continued to decay with time when the temperature was kept constant at 90 °C.

temperature of these samples was measured at 130 °C. After that, to obtain the multi-domain structure on the $BaTiO_3$ (0 0 1) surface for the surface potential measurements, the sample was annealed in air at 110 °C for 2 h, prior to the ferroelectric and paraelectric phases transitions at the 130 °C Curie temperature. The $BaTiO_3$ single crystal has a typical tetragonal perovskite structure at room temperature. The complex polarized domain structure was comprised of the domains containing ***a***, $\boldsymbol{c}^+$ and $\boldsymbol{c}^-$ domains, and boundaries between these domains. It is possible to identify the direction of spontaneous polarization in ferroelectrics using SKPFM by measuring the surface potential due to the charge with respect to different polarization on the $BaTiO_3$ (0 0 1) plane.

The experiments were carried out with the Digital Instruments Dimension V SPM system. Scanning surface potential microscopy was performed in this paper. During the surface potential measurements W_2C-coated tip (NSG01/W_2C, NT-MDT, Russia) was used. These experiments were performed at 135 kHz, just below the cantilevers' resonance frequency of 150 kHz. The lift scan height in the interleave control was set to 100 nm. An oscillating voltage $V_{ac}\cos\omega t$ was applied directly to the cantilever tip to measure the surface potential. In these studies the driving voltage, V_{ac}, was set at 3 V. The scan rate was 0.6 Hz with 256 scan lines, thus it took almost 14 min to finish the whole image capture. A hot plate was equipped onto the sample stage to achieve the control of the sample temperature during the experiments. The commercial hot plate provides a temperature range from ambient to 250 °C. The Lakeshore 332 temperature controller was used to drive the hot plate and realize accurate temperature measurements and control with ±0.5 °C accuracy. The heating rate was keep at 100 °C/min.

In this work, the surface potential distribution of the nanoscale domain structures was measured when decreasing the temperature of the ferroelectric phase. The sample was first kept in air at room temperature. Then a heat treatment in which the sample temperature was increased from RT to 115 °C was conducted. After 30 min stabilization, temperature decrease from 115 °C to 90 °C was controlled using the hot plate, and SKPFM was used to capture the surface potential evolution.

3. Results and discussion

Fig. 1 shows the surface potential distribution of the 90° ***a***–***c*** domain structure before and after cooling. Fig. 1(a) is the AFM topography image of the 90° ***a***–***c*** domain structure with respect to the (0 0 1) $BaTiO_3$ surface with a 200 nm Z scale at 115 °C. Since the ***c*** domain has a polarization vector pointing either upward ($\boldsymbol{c}^+$) or downward ($\boldsymbol{c}^-$) with respect to the (0 0 1) plane, the polarization charge is generated on the surface. The dark regions within the ***c*** domain have a negative potential and correspond to the $\boldsymbol{c}^-$ domains, while the surrounding bright regions have a positive potential and correspond to the $\boldsymbol{c}^+$ domains. The ***a*** domain polarization vector is in the (0 0 1) plane and thus has no surface charge, so its contrast is in-between the $\boldsymbol{c}^+$ and $\boldsymbol{c}^-$ domains. The corrugated topography is attributed to the adjacent ***a*** and ***c*** domains, induced by the 0.6° orientation difference at room temperature. The observed straight lines on the surface were assigned to the 90° ***a***–***c*** domain walls on the (0 0 1) surface. Although there is no corrugation on the surface, the 180° ***c***–***c*** domain wall obviously appears as curved lines in the surface potential image. It is observed that the typical ***c*** domain stripe size is about 10 μm on the (0 0 1) surface. The domain wall width is estimated at 100 nm from the surface potential image in Fig. 1(b).

Upon decreasing the sample temperature to 90 °C, the image topography did not change significantly, only exhibiting a slight change of the ***a***–***c*** domain tilt angle. Neither ***a***, nor ***c*** domain potentials change was observed. However, the potential distribution near the 90° ***a***–***c*** domain walls underwent a significant change. The corresponding surface potential image at 115 °C is shown in Fig. 1(b). The ***c*** domain zones show nearly positive high surface potential distribution on the stripes with only quite tiny negative zone around them. After cooling to 90 °C, the surface potential image was immediately captured. A higher broad potential barrier burst at the 90° ***a***–***c*** domain wall area (0.6 V Z scale) is shown in Fig. 1(c). The height reached 200 mV, while the width of the domain wall was up to 1–3 μm. Cross section profiles between 90 °C and 115 °C were compared to clarify the location of the potential barrier. The circled area showing a large drop of the surface potential was induced by the surface impurity, used as a reference mark. Fig. 2(a) and (b) shows the surface potential profiles across the marked line acquired at 115 °C and immediately after cooling to 90 °C, respectively. It shows that the potential barrier embraces the 90° ***a***–***c*** domain wall and exactly matches the domain wall in Fig. 2(c). The increased domain wall potential contrast is transient. At 90 °C decay of the potential barrier continues, as shown in Fig. 3, where both the height and the width were reduced. At the first 45 min the domain wall potential decayed quite fast and then slowed down. It shows a large instability after a few dozen degrees change in temperature. Further, after 120 min the domain wall potential barrier disappeared. Quantitative analysis of the surface potential decay process shows that the domain wall high potential relaxes, following an exponential time dependence, given by $V = V_0 + B\exp(-t/\tau)$, where τ is the associated relaxation time constant. The time constants extracted from the data is $\tau = 30.6$ s. The decay rate became slower with time, as seen in Fig. 4, until the domain wall barrier disappeared completely. It followed conventional charge diffusion process. The high domain wall potential can be fully recovered when given sufficient time.

In ferroelectrics, domain polarization would induce surface charges [26]. The surface charges play a significant role in the ferroelectric domain performance [26]. Therefore, the surface screening charges should be taken into account in the ferroelectrics characterization. Previous studies have already shown that screening plays a significant role in the polarization reversal processes and to a large extent determines the stability of the domain structures in

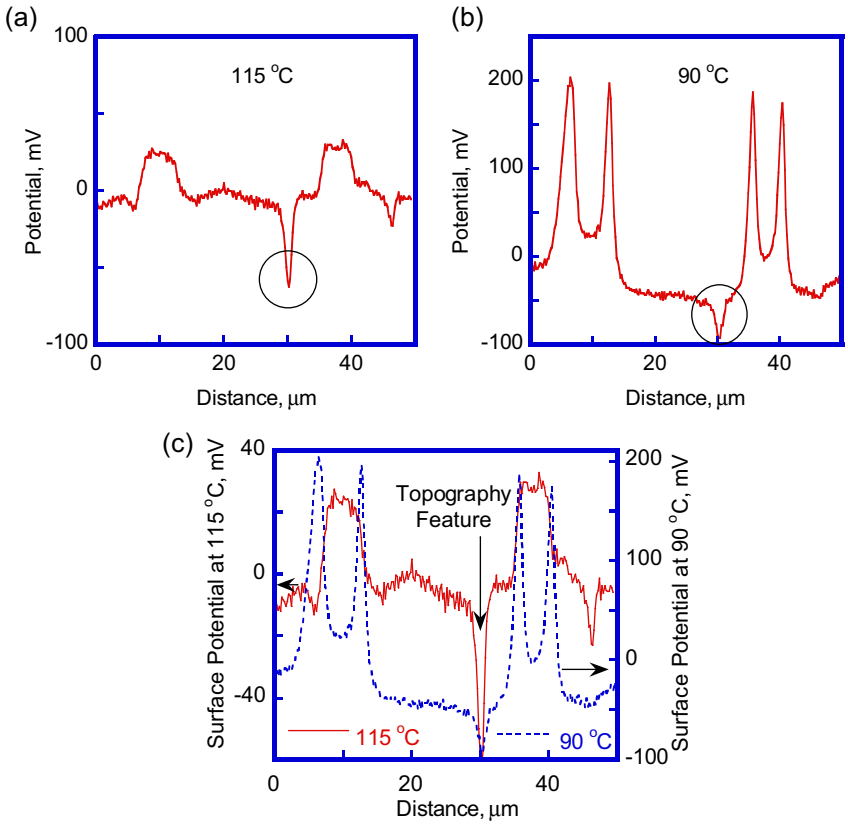

Fig. 2. (a) The surface potential scan line at 115 °C. Here, the circled area is a topography feature used as a reference mark; (b) the surface potential at the same scan line acquired immediately after cooling to 90 °C; (c) the surface potentials comparison between 115 °C and 90 °C showing an alignment at the domain wall.

ferroelectrics [27,28]. This temperature field-induced domain wall potential stability transition to metastability and then back to stability provides a charge migration model across the domain wall. Charge trapping and diffusion at the domain walls cause a large surface potential change around the domain walls. Since at the top of the ***c*** domain surface the polarization vector points either upward (c^+) or downward (c^-) with respect to the (0 0 1) plane, the polarization charge is generated on the surface. However, for the ***a*** domain, its vector is in the (0 0 1) plane and thus has no surface charge. Thermal activation is inclined to cause the surface charge migration with the temperature change. The polarization intensity goes down with the increasing temperature of the ferroelectric phase [26]. Then, after cooling, the domain polarization was enhanced to a certain extent, thus the original screening charge was not sufficient to compensate the new polarization state, inducing charge spreading on the surface. The surface charge density was also increased. The ***a***–***c*** domain wall suffers a topological misfit due to the transition of the ***a*** and ***c*** domains, thus it acts as a natural trap for charges, holes, oxygen vacancies, etc. During the surface charge migration the domain wall acts as a trap, attracting charges. Thus, the screening charges are inclined to assemble on the sample surface.

SKPFM utilizes a nulling method and measures the sample effective surface voltage by adjusting the tip bias voltage [29], thus as

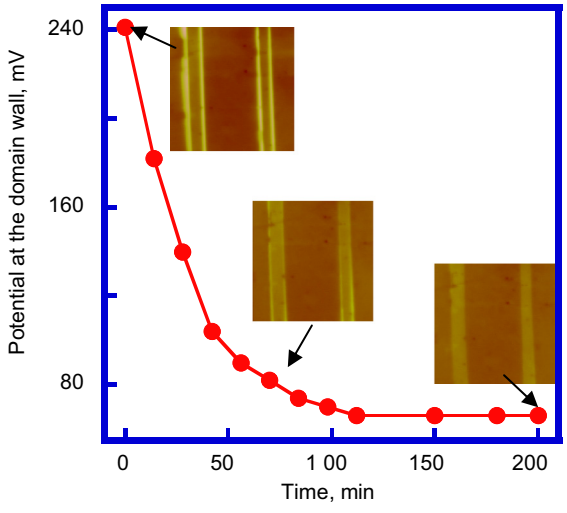

Fig. 3. Time dependence of the domain wall potential at 90 °C demonstrating the potential barrier decay.

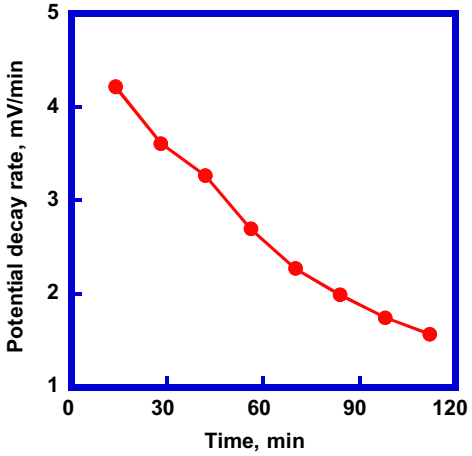

Fig. 4. Time dependence of the potential barrier decay rate.

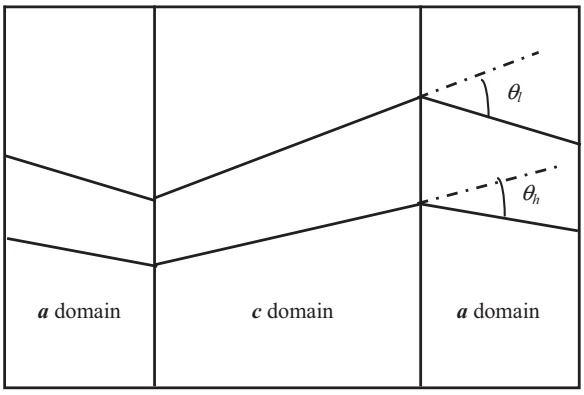

Fig. 5. Schematic of a typical $BaTiO_3$ ***a***–***c***–***a*** domain pattern at low and high temperatures showing a difference in the ***a***–***c*** domain angles with temperature variation. (θ_l and θ_h represent low and high temperature domain angles, respectively.)

it feels a minimum electric force from the sample, the output signal from the instrument was inverted to reflect the actual surface polarity. In our experiments, the work function acquired from the domain wall surface potential [30] and the signal inversion gave sufficient evidence that the 90° domain wall is inclined to assemble the mobile charges. The observed high potential at the domain wall indicates that there are charges emerging around it. To a certain extent, the domain wall inhibits surface charges motion and, consequently, results in the surface potential enhancement. Then, with the exposure to the surrounding environment, the assembled surface charges at the domain wall are neutralized by the surface adsorbates to reduce the instantaneous high energy at the domain wall area. Thus, the ***c*** domain surface charge diffusion plays a major part in the process.

In addition, the appearance of the high potential zone could be due to the material properties changes in the area of the main domain wall. The wall is found to be quite narrow, thus the polarization change at the boundary is abrupt [15]. With the abrupt change of the polarization direction across the wall, the inhomogeneous stress always exists in the vicinity of the domain wall due to the external field effect [31]. Thus, these highly stressed and distorted regions around the domain wall could have different physical properties from the bulk values [32]. The domain wall width could also change at the domain wall zone. Jun et al. performed high resolution transmission electron microscopy and showed that with the increasing temperature, the areas of $BaTiO_3$ nanoparticle domains increased and the domain walls became narrower, however, the walls did not move during the heating and cooling cycles, up to 200 °C [33]. The fringe bending due to the phase shift in the domain wall with varying temperature was also observed [34]. Rao and Wang's simulation results also showed that under the applied electric field, the domain wall would broaden and serve as an embryo for the new field-induced phase, producing large reversible strain [35]. The broad change of the domain wall width and strain after decreasing the temperature may be associated with the surface effects. Temperature fluctuations induce strain, accompanied by the domain wall polarization direction change, resulting in a different average corrugation angle between the ***a*** and ***c*** domains, shown schematically in Fig. 5. The angle change has already been reported by Kalinin et al. [26], where at relatively high temperatures the angle became smaller. The presence of the 90° domain walls strain inhibits the motion of surface charges, contributing to the mobilized surface charges accumulation.

Thus, the thermodynamically high potential behavior in the vicinity of the domain wall or boundary is significantly affected by the combination of several effects, i.e.: (1) surface charge mobility, (2) domain walls character, (3) domain pattern, (4) polarization and strain change across the wall. For the coupling effect, after decreasing the temperature, the surface screening charges and their mobility play a dominant role in the described experiments. Besides, polarization and strain changes across the wall induce a large physical change of the material, also contributing to the appearance of the high potential zone.

4. Conclusions

In summary, SKPFM was employed to study the surface potential evolution at the 90° ***a***–***c*** domain wall on the (0 0 1) $BaTiO_3$ single crystal surface due to decreasing temperature. A strong temperature effect on the surface potential of the $BaTiO_3$ domain wall was found. A high broad domain wall potential barrier appears at the 90° ***a***–***c*** domain walls immediately after decreasing the ferroelectric phase temperature. The observed potential barriers were not stable and gradually decayed with time. The temperature decrease induced high potential barrier at the 90° ***a***–***c*** domain wall, which mainly relies on the ***c*** domain surface charge migration, helped by the increasing domain polarity and the subsequent charges trapped at the 90° ***a***–***c*** domain twin walls. The high domain wall potential barrier decay followed the screening charges adsorbed on the surface. Direct observation of the 90° ***a***–***c*** domain wall high potential zone gives convincing evidence that the fine tilt of the domain wall polarization would induce strain in the domain wall areas. The polarization and strain changes across the wall induce large physical material changes, which should also be taken into account.

Acknowledgments

The authors acknowledge support from the National Natural Science Foundation of China under grant 51072021, the Beijing Municipal Commission of Education under the YB20091000801 grant and the Program for the Changjiang Scholars and the Innovative Research Team in the University (IRT1207).

References

[1] Y.H. Shin, I. Grinberg, I.W. Chen, A.M. Rappe, Nature 449 (2007) 881.
[2] S.S.N. Bharadwaja, D. Damjanovic, N. Setter, Ferroelectrics 303 (2004) 59.
[3] S. Farokhipoor, B. Noheda, Phys. Rev. Lett. 107 (2011) 127601.
[4] N. Bassiri-Gharb, I. Fujii, E. Hong, S. Trolier-McKinstry, D.V. Taylor, D. Damjanovic, J. Electroceram. 19 (2007) 49.
[5] H. Chaib, F. Schlaphof, T. Otto, L.M. Eng, J. Phys.: Condens. Matter 15 (2003) 8927.
[6] W. Li, M. Alexe, Appl. Phys. Lett. 91 (2007) 262903.
[7] R. Pérez, J.E. García, A. Albareda, V. Gomis, D.A. Ochoa, Mech. Mater. 42 (2010) 374.
[8] S. Lisenkov, I. Ponomareva, L. Bellaiche, Phys. Rev. B: Condens. Matter 79 (2009) 024101.
[9] P. Marton, T. Shimada, T. Kitamura, C. Elsasser, Phys. Rev. B: Condens. Matter 83 (2011) 064110.
[10] B. Meyer, D. Vanderbilt, Phys. Rev. B: Condens. Matter 65 (2002) 104111.
[11] X. Zhang, T. Hashimoto, D.C. Joy, Appl. Phys. Lett. 60 (1992) 784.
[12] J. Hlinka, P. Márton, Phys. Rev. B: Condens. Matter 74 (2006) 104104.
[13] N. Floquet, C. Valot, Ferroelectrics 234 (1999) 107.
[14] L.M. Eng, H.J. Guntherodt, Ferroelectrics 236 (2000) 35.
[15] C.L. Jia, S.B. Mi, K. Urban, I. Vrejoiu, M. Alexe, D. Hesse, Nat. Mater. 7 (2008) 57.
[16] S.V. Kalinin, D.A. Bonnell, Appl. Phys. Lett. 78 (2001) 1116.
[17] S. Shin, J. Baek, J.W. Hong, Z.G. Khim, J. Appl. Phys. 96 (2004) 4372.
[18] R. Shao, M.P. Nikiforov, D.A. Bonnell, Appl. Phys. Lett. 89 (2006) 112904.
[19] Q. Dai, J. Hu, M. Salmeron, J. Phys. Chem. B 101 (1997) 1994.
[20] M. Luna, J. Colchero, A.M. Baro, J. Phys. Chem. B 103 (1999) 9576.
[21] M. Luna, J. Colchero, A. Gil, J. Go'mez-Herrero, A.M. Baro, Appl. Surf. Sci. 157 (2000) 393.
[22] A. Verdaguer, M. Cardellach, J. Fraxedas, J. Chem. Phys. 129 (2008) 174705.
[23] D.B. Li, M.H. Zhao, J. Garra, A.M. Kolpak, A.M. Rappe, D.A. Bonnell, J.M. Vohs, Nat. Mater. 7 (2008) 473.
[24] Q. Zhang, C.H. Kim, Y.H. Jang, H.J. Hwang, J.H. Cho, Appl. Phys. Lett. 96 (2010) 152901.
[25] Y. Kim, M. Park, S. Buhlmann, S. Hong, Y.K. Kim, H. Ko, J. Kim, K. No, J. Appl. Phys. 107 (2010) 054103.
[26] S.V. Kalinin, C.Y. Johnson, D.A. Bonnell, J. Appl. Phys. 91 (2002) 3816.

[27] D.Y. He, L.J. Qiao, A.A. Volinsky, Y. Bai, L.Q. Guo, Phys. Rev. B: Condens. Matter 84 (2011) 024101.
[28] D.Y. He, L.J. Qiao, Alex A. Volinsky, J. Appl. Phys. 110 (2011) 074104.
[29] S.V. Kalinin, D.A. Bonnell, Phys. Rev. B: Condens. Matter 63 (2001) 125411.
[30] M. Femenia, C. Canalias, J. Pan, C. Leygraf, J. Electrochem. Soc. 150 (2003) B274.
[31] E.A. Eliseev, A.N. Morozovska, S.V. Kalinin, Y.l. Li, J. Shen, M.D. Glinchuk, L.Q. Chen, V. Gopalan, J. Appl. Phys. 106 (2009) 084192.
[32] D.A. Scrymgeour, V. Gopalan, Phys. Rev. B: Condens. Matter 72 (2005) 024103.
[33] B.E. Jun, B.K. Moon, J.S. Kim, J.H. Jeong, B.C. Choi, S.T. Jeong, Y.I. Kim, K.S. Ryu, J. Korean Phys. Soc. 55 (2009) 2543.
[34] K. Uchino, E. Sadanaga, T. Hirose, J. Am. Ceram. Soc. 72 (1989) 1555.
[35] W.F. Rao, Y.U. Wang, Appl. Phys. Lett. 90 (2007) 041915.